Hindawi
Advances in Materials Science and Engineering
Volume 2023, Article ID 3232992, 18 pages
https://doi.org/10.1155/2023/3232992

Research Article

Study on Mechanical Properties of Concrete-Filled Steel Tubular Members under Axial Tension

Huaguo Gao,[1,2,3] Lingxin Zhang,[1,2] Xiuchun Wang,[3] Renjie Sun,[3] Qingli Wang,[3] and Lu Yang[4]

[1]*Institute of Engineering Mechanics, China Earthquake Administration, Harbin 150080, China*
[2]*Key Laboratory of Earthquake Engineering and Engineering Vibration of China Earthquake Administration, Harbin 150080, China*
[3]*University of Science and Technology Liaoning, Anshan 114051, China*
[4]*Shenyang University of Technology, Shenyang 110000, China*

Correspondence should be addressed to Lingxin Zhang; civilengineering@ustl.edu.cn

Received 19 November 2021; Revised 7 July 2022; Accepted 13 July 2022; Published 24 April 2023

Academic Editor: Junjie Wang

At present, the concrete-filled steel tube structure has been widely used in various practical projects. Due to the low tensile strength of the core concrete of round steel tube concrete (CFST) specimens, the axial tensile performance of CFST specimens is far from superior to its compressive performance. However, in practical projects, the concrete-filled steel tube members bearing tensile load often appear. In order to study the axial tensile properties of CFST specimens, the axial tensile tests of 5 CFST specimens and 1 pure steel tube specimen were carried out with steel tube diameter and concrete strength as variation parameters. The results show that the bearing capacity of CFST specimens is increased by 7.5%–16.3% compared with that of pure steel tube specimens with the same cross-sectional area, mainly because the core concrete limits the circumferential shrinkage of the outer steel tube. The larger the cross-sectional area of CFST specimens is, the higher the bearing capacity is. In this paper, the stress-strain relationship and the overall failure mode of CFST members under tensile force are studied, and the deformation characteristics and stress of steel pipe and core concrete are analyzed, which is expected to provide a reference for the application of CFST specimens in practical engineering.

1. Introduction

The essence of the concrete-filled steel tube (CFST) component is the restraining effect of the outer steel tube on the core concrete, which produces an excellent combination effect between the two materials, thus showing many advantages. Because the compressive capacity of concrete materials is much higher than its tensile capacity, it is mainly used as compression members in actual projects, it is rarely used in tension members, and there are relatively few related studies. However, when it is used as the bottom side column of high-rise building under wind load or earthquake load, the base and bracket of a large structure under horizontal wind load, and the tie rod in a truss structure, the member is in the tension state. At the same time, the stress mode of concrete-filled steel tubular members in eccentric tension is similar to that of compression bending members. The study on the tensile bending performance of CFST members has certain reference significance for us to understand the compression bending performance of concrete-filled steel tubular members. The axial tensile and eccentric tensile properties of concrete-filled steel tubular (CFST) are one of the most basic mechanical properties. Since the research team will also carry out the tensile performance test of CFRP concrete-filled steel tubular (CFST) in the later stage, the research on the axial tensile properties of ordinary CFST is also to lay a foundation for the later research on a series of related properties of CFRP concrete-filled steel tubular (CFST). Therefore, it is very important to study the mechanical properties of CFST components under tensile load.

Compared with previous studies, this paper finds that the bearing capacity of CFST will be improved, and the ductility will be reduced.

Han [1] made a systematic study about the concrete-filled steel tubular structures theory. Some scholars have studied the axial tensile properties of concrete-filled steel tubular specimens, and the authors of [2] conducted an experimental study on the tensile properties of concrete-filled square steel tubular and proposed that the improvement of tensile stiffness was the comprehensive result of finite stiffness effect and tensile stiffness effect. The design formula and analysis were a model of circular CFST under axial tension put forward by Xu et al. [3]. Hua et al. [4], Ying [5], Wang et al. [6], Han et al. [7] conducted detailed research and analysis on the axial tensile properties of concrete-filled steel tube members through experimental research and finite element analysis. The effects of material properties, steel content, cross-sectional form, concrete shrinkage, and carbon fibre reinforced plastics (CFRP) reinforcement on the axial tensile properties of the specimens were discussed. Li et al. [8] have studied the performance of concrete-filled steel tubes subjected to eccentric tension. Wang et al. [9] did some research on the behavior of CFRP externally reinforced circular CFST members under combined tension and bending. Experimental research and finite element analysis were carried out on the axial tension and tension-bending performance of hollow sandwich steel tube concrete and reinforced steel tube concrete, and the corresponding calculation methods of bearing capacity and stiffness were proposed [10, 11]. Ye et al. [12] evaluated the variation of tensile strength and studied the tensile properties of circular CFST members with small gaps. Han et al. [13] and Zhou et al. [2] studied the mechanical behavior of concrete-filled steel tubes (CFST) under axial tension, established the finite element model of axial tension of concrete-filled steel tubular, and carried out mechanical analysis and parameter research. Chen et al. [14] carried out a series of axial tensile tests on concrete-filled steel tubular with reinforcement or angle steel. The properties and strength of concrete-filled steel tubular with reinforcement or angle steel under axial tension were studied. Zhou et al. [15] studied the mechanical behavior of circular concrete-filled steel tubular (CCFTS) under axial tension. The test results showed that the tensile strength of CCFTS was approximately 10.2% larger than that of hollow tubes. This stiffness and strength enhancement should be considered in typical static and dynamic analyses of structures using CCFT members subjected to tension to provide more accurate results. Qiao et al. [16] studied the seismic behavior of specially shaped concrete-filled tube (CFT) columns with multiple cavities under axial tension or axial compression. The results showed that the compression-flexure test specimen showed lower yield damage, higher bearing capacity, and superior seismic performance relative to the tension-flexure test specimen. Han et al. [13] carried out the axial tension test study of 18 concrete-filled steel tube specimens, established the relevant finite element analysis model, then deeply analyzed the axial tension force mechanism of the concrete-filled steel tube member, and summarized the formula for calculating the bearing capacity of the shaft in relation to the steel rate.

$$N_u = (1.1 - 0.4\alpha) f_y A_s, \tag{1}$$

where N_u is the axial tension capacity, α is the steel content, f_y is the yield strength of steel tube, and A_s is the cross-sectional area of steel tube.

Through the above literature research, compared with the mechanical properties of other CFST members, there are few studies on its axial tensile properties, and the constitutive relationship curve of the steel used in the finite element simulation is different from the relationship curve obtained by the actual tension of the steel pipe. The calculation of steel content in formula (1) is complicated. Therefore, on the basis of the existing research, this paper analyzes in detail the deformation and stress characteristics of the outer steel pipe and the core concrete during the test, and adjusts the existing steel constitutive relationship on the basis of the actual tensile curve of the steel pipe, and adopts finite element method for parameter analysis. Finally, a simplified calculation formula for the axial tension bearing capacity related to the wall thickness and outer diameter ratio is proposed. It is expected to provide a reference for quickly calculating the bearing capacity of this type of member in engineering practice.

2. Test Overview

2.1. Specimen Design. In this experiment, a total of 1 pure steel tube and 5 circular steel tube concrete members was designed and manufactured. The detailed parameters of the test piece are shown in Table 1, where α is the steel content, which can be calculated according to formula (2). The length of the test piece is 460 mm. The detailed dimensions of the end plates and stiffeners of the test piece are shown in Figure 1. The front number in the serial number is the outer diameter of the steel tube, the back number represents the strength grades of the core concrete of the specimen as C30, C40, and C50, and the number 0 represents that the specimen is a pure steel pipe specimen.

$$\alpha = \frac{A_s}{A_c}, \tag{2}$$

where A_s is the cross-sectional area of the steel, and A_c is the cross-sectional area of the concrete.

2.2. Material Properties Experiment

2.2.1. Steel Performance. The model of the steel used in the production of the test piece is Q235 according to the relevant regulations in "Tensile Test of Metallic Materials Part 1: Room Temperature Test Method" GB/T 228.1 [17]. Three test specimens are cut out from the steel used in the test piece. Tensile specimens were tested for the material properties of the steel, and the relevant material properties of the steel are measured in Table 2. In the table, f_y is the yield strength, f_u is the ultimate strength, E_s is the modulus of elasticity, ν_s is the Poisson's ratio, and δ' is the elongation. The tensile specimen is shown in Figures 2(a) and 2(b).

Table 1: Specimen parameter.

Number	Diameter (mm)	Tube thickness (mm)	α	$f_{cu\cdot k}$ (MPa)
1	89	3.5	0.178	40
2	114	3.5	0.135	40
3	139	3.5	0.109	40
4	114	3.5	0.135	30
5	114	3.5	0.135	50
6	114	3.5	—	—

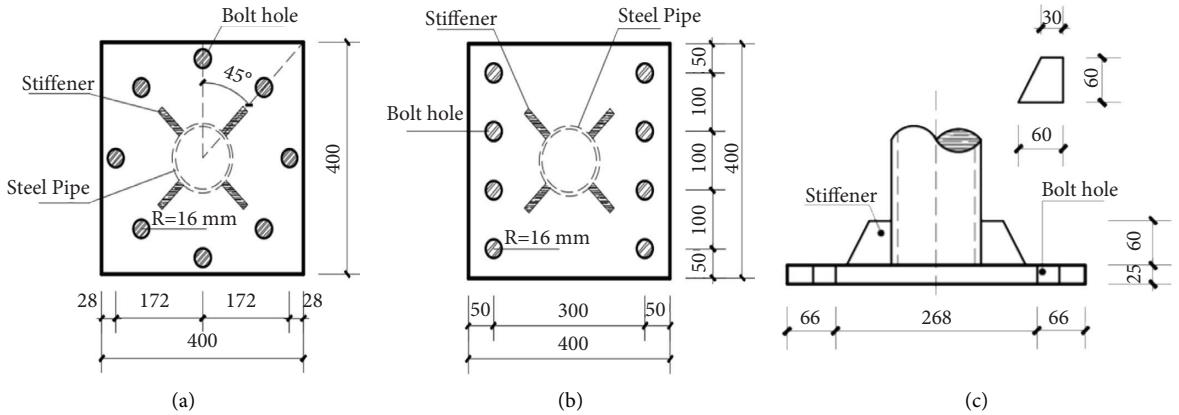

Figure 1: Sizes of specimens (unit: mm): (a) upper end plate, (b) lower end plate, and (c) stiffener.

Table 2: Properties of steel tube.

f_y (MPa)	f_u (MPa)	E_s (GPa)	v_s	δ' (%)
305.6	447	199.67	0.29	29.7

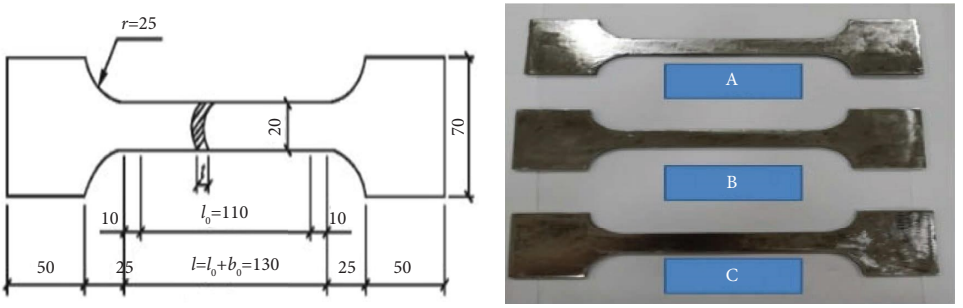

Figure 2: Steel tensile test piece production: (a) tensile specimen size and (b) tensile specimen.

According to the relevant regulations in the "Standard for Test Methods for Physical and Mechanical Properties of Concrete" GB/T50081 [18], the compressive strength test of standard concrete test blocks is carried out, and the compressive strength of three strength concretes is measured. The elastic modulus E_c can be calculated by formula (3), and Poisson's ratio v_c is 0.2. The relevant material properties of concrete can be gotten from Table 3.

$$E_c = 4700\sqrt{f_c'}, \tag{3}$$

where f_c is the standard value of the compressive strength of the concrete cylinder, which can be taken according to the literature.

2.2.2. Concrete Performance. In order to prevent the internal strain gauge from falling off, the method of manual mixing is used in the mixing process, that is, placing a vibrator inside while pouring concrete, and hammering it outside the steel pipe with a leather hammer, and the mix proportion is shown in Table 4. In the table, C is grade 42.5 ordinary Portland cement, G is natural medium sand, the fineness

Table 3: Properties of concrete.

Strength level	C30	C40	C50
$f_{cu\cdot k}$ (MPa)	31.3	39.6	52.0
E_c (GPa)	23.50	26.96	30.28

modulus is 2.5, S is gravel coarse aggregate with the maximum particle size of 25 mm, W is tap water, and SP is hydroxy acid water reducing agent. The water-cement ratio of three strength concrete is 0.487, 0.395, and 0.349, respectively.

In this paper, a total of 10 standard concrete test blocks are made, 3 test blocks are configured for each strength of concrete, and another test block with a strength grade of C40 is made. The configuration of test block is shown in Figure 3(a). After the test block is demoulded, the test block is placed in the same environment as the concrete-filled steel tube, that is, the test block is watered, and the same watering frequency is used for curing until the test is carried out, and the press is used to test each test block.

The concrete test blocks were tested for compressive strength, as shown in Figure 3(b). Now, the compressive strength of each test block is listed in Table 5. Since the test was carried out immediately after the 28 d curing period of concrete, the concrete strength before the test was not measured. The relevant data of 28 d concrete in Table 5 can be used directly.

2.3. Test Piece Production. Cut the steel tube, end plate, and stiffener according to the design size of the test piece. First, complete the welding of the steel pipe and the lower end plate, and paste the horizontal and vertical strain gauges on the inner wall of the steel pipe at a position 1/3L from the upper port. Drill a 5 mm hole between the ribs to connect the strain gauge. Connect the wires throughout. The internal strain gauge treatment is shown in Figure 4. After the concrete is poured, the port is ground flat, and the upper-end plate and the stiffener are welded. A small hole with a radius of 15 mm is reserved at the center of the upper-end plate for water injection curing of the concrete.

After the test piece is made, in order to prevent the corrosion of the steel pipe, the outside of the test piece shall be painted. Before the test, in order to solve the void phenomenon of the end plate caused by the shrinkage of the concrete, after the concrete curing period, epoxy is injected into the water injection hole of the upper-end plate resin fills the gap between the concrete shrinkage and the end plate. The sample before loading is shown in Figure 5.

2.4. Test Device and Measurement. The test was carried out on a 3000 kN electro-hydraulic servo short column eccentric compression testing machine in the structural engineering laboratory of University of Science and Technology Liaoning, and the manufacturer of the equipment is Jilin Jinli Test Technology Co., LTD. During the test, place the test piece on the operating platform of the testing machine, and align the centers of the upper and lower end plates with the centroids of the test device base and the force sensor, and

Table 4: Concrete material consumption table.

Strength grade	Material consumption per cubic meter (kg/m^3)				
	C	S	G	W	SP
C30	380	1198	648	185	3.9
C40	460	1210	590	182	4.2
C50	510	1220	545	178	4.5

place them vertically to ensure that the bolt holes are aligned. The upper and lower end plates are connected with the testing machine through $8 * 12.9$ grade high-strength bolts. The boundary conditions are approximately completely fixed, and the test loading device is shown in Figure 6.

In order to accurately measure the deformation of the test specimen, 3 measuring points are arranged at the mid-span section with an interval of 120°. Each measuring point is pasted with two strain gauges in the horizontal and vertical directions. The steel pipe is at a position 1/3L from the upper and lower end plates. Two measuring points are set on the outer wall, and each measuring point is pasted with two horizontal and vertical strain gauges to measure the strain at 1/3L of the test piece. In order to study the difference in strain at the same point on the inner and outer surfaces of the steel pipe, paste two horizontal and vertical strain gauges on the inner wall of the 1/3L section. Finally, paste two horizontal and vertical strain gauges on the stiffeners at both ends to study the strain at the stiffener. The layout of the strain gauges is shown in Figure 7.

Axial force is measured by a spoke force sensor. The overall displacement of the test piece is measured by a 100 mm range thimble displacement meter at the loading end plate. Two sizes are spot welded at the upper and lower 1/3L of the test piece before the test. It is a steel sheet of 20 mm × 40 mm (spot welding is only for fixing the steel sheet, and the influence on the steel pipe is negligible), and two thimble type displacement meters with a range of 50 mm are arranged on the two steel sheets, respectively, and the measurement is on the middle 1/3L of the test piece. The layout of the displacement meter is shown in Figure 8(a).

2.5. Acquisition System and Loading System. Displacement loading was adopted in the test with a loading rate of 1 mm/min. During the test, the tension was measured by a spokes force sensor with a range of 3000 kN, and the stress, strain, and displacement were simultaneously collected by the DH3816H static stress and strain tester produced by Donghua Testing Company, as shown in Figure 8(b). Using the same acquisition device to collect experimental data can ensure that different data are collected at the same time and maintain a one-to-one correspondence relationship. The data acquisition frequency is set to 1 Hz.

3. Analysis of Test Results

3.1. Test Phenomenon and Failure Mode. At the beginning of loading, the specimen is the elastic range, and the deformation of the specimen is small, so the experimental

(a) (b)

Figure 3: Concrete test block configuration diagram: (a) block configuration and (b) compression test.

Table 5: Test block compressive strength measured table.

Configuration grade	f_{cu} (MPa)			
	Block 1	Block 2	Block 3	Average value
C30	34	31	29	31.3
C40	42	39	38	39.6
C50	49	52	55	52.0

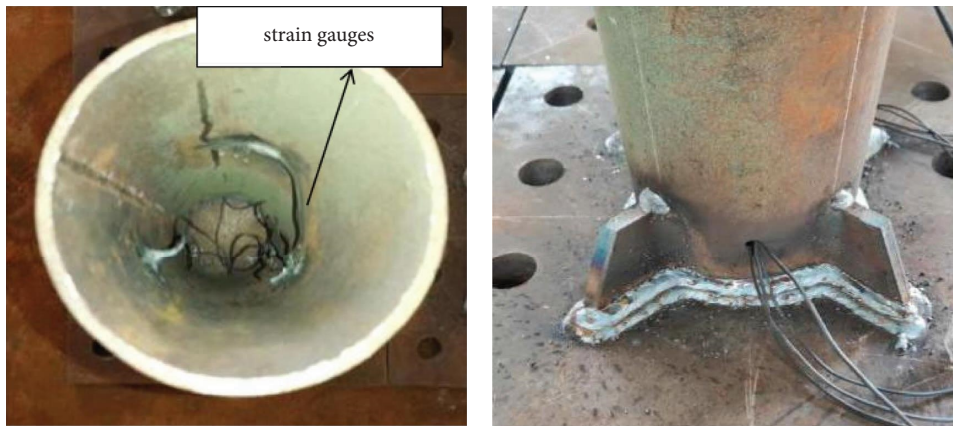

(a) (b)

Figure 4: Sticking of strain gauges on inner wall: (a) arrangement of inner strain gauges and (b) wire handling method.

phenomenon is not obvious. As the axial force increases, the specimen has a slight "snapping" sound, and the spray paint on some areas of the outer surface is torn. When the axial tensile force reaches about 80% of the ultimate bearing capacity of the specimen (the 114-40 specimen reaches 37.1 t at this time, and the ultimate bearing capacity of the specimen is 47.6 T), the growth rate of specimen displacement is accelerated, and the specimen enters the elastic-plastic stage. The accelerated deformation results in cracks of AB glue attached to the outer surface of strain gauge. As the load increases, the test piece enters the strengthening stage, and the longitudinal deformation of the test piece is large, and the outer steel pipe shrinks laterally, causing some strain gauges to fall off. When the specimen is damaged, cracks appear at one point of the outer steel pipe, and the bearing capacity decreases, and the cracks gradually extend along the circumferential direction. Finally, the specimen fractures and the test end. The damage of the specimen after the test is shown in Figure 9.

Through comparative analysis, it is concluded that there are three types of failures of the specimen: 1. the midspan section damages (114-0). Due to the absence of the restraint effect of the core concrete, the midspan section of the specimen exhibits obvious diameter shrinkage, and then damage occurs. 2. The junction between the top of the stiffener and the steel pipe is damaged (139-40). Due to the increase in pipe diameter but the same wall thickness, the stress concentration at this position is more obvious, and the steel pipe outside the section is weaker due to welding, so damage occurs. 3. Damage section is near to the 1/3L section (89-40, 114-30, 114-40, 114-50). Since the transverse deformation of the

Figure 5: Specimens before loading.

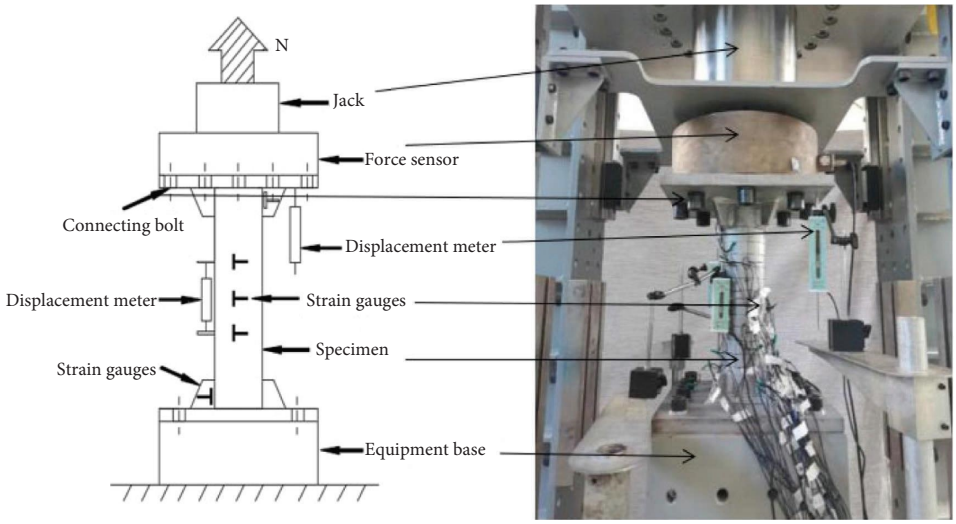

Figure 6: Experimental setup.

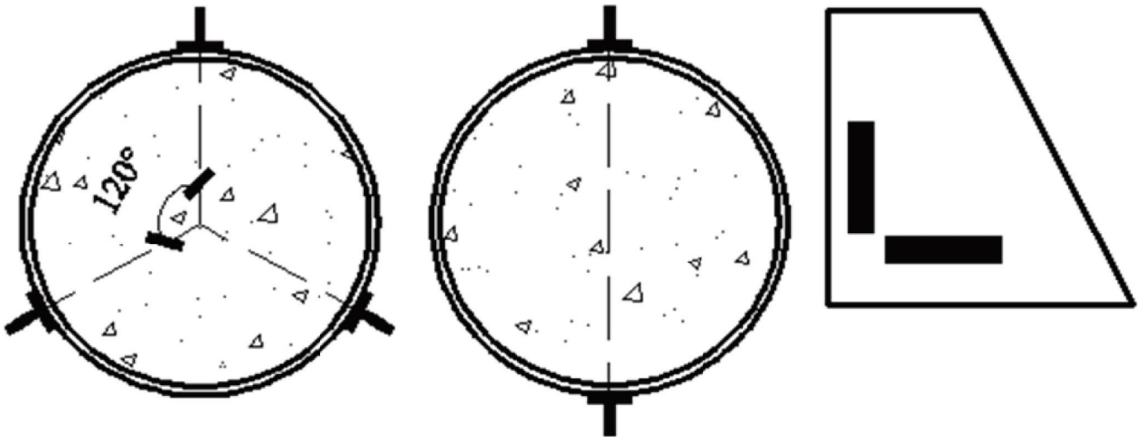

Figure 7: Distribution of strain gauge: (a) 1/2L section, (b) 1/3L section, and (c) stiffener.

specimen is constrained by the core concrete, the fracture position should be related to the damage position of the concrete, and the concrete appears after the crack, and the position of the crack no longer provides hoop restraint, resulting in stress concentration of the outer steel pipe at this position and subsequent failure.

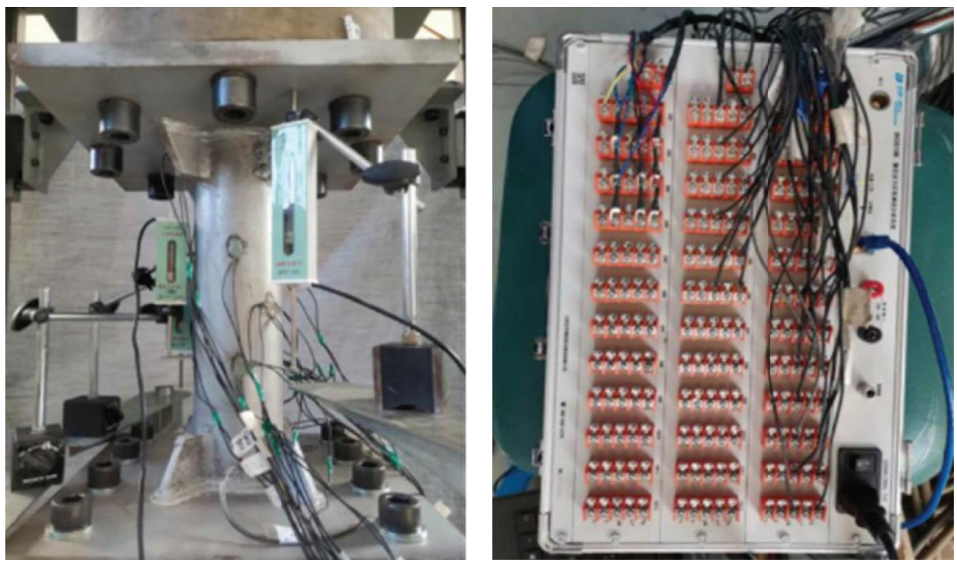

(a) (b)

Figure 8: Displacement meter layout and data acquisition device: (a) displacement gauge layout drawing and (b) data acquisition unit.

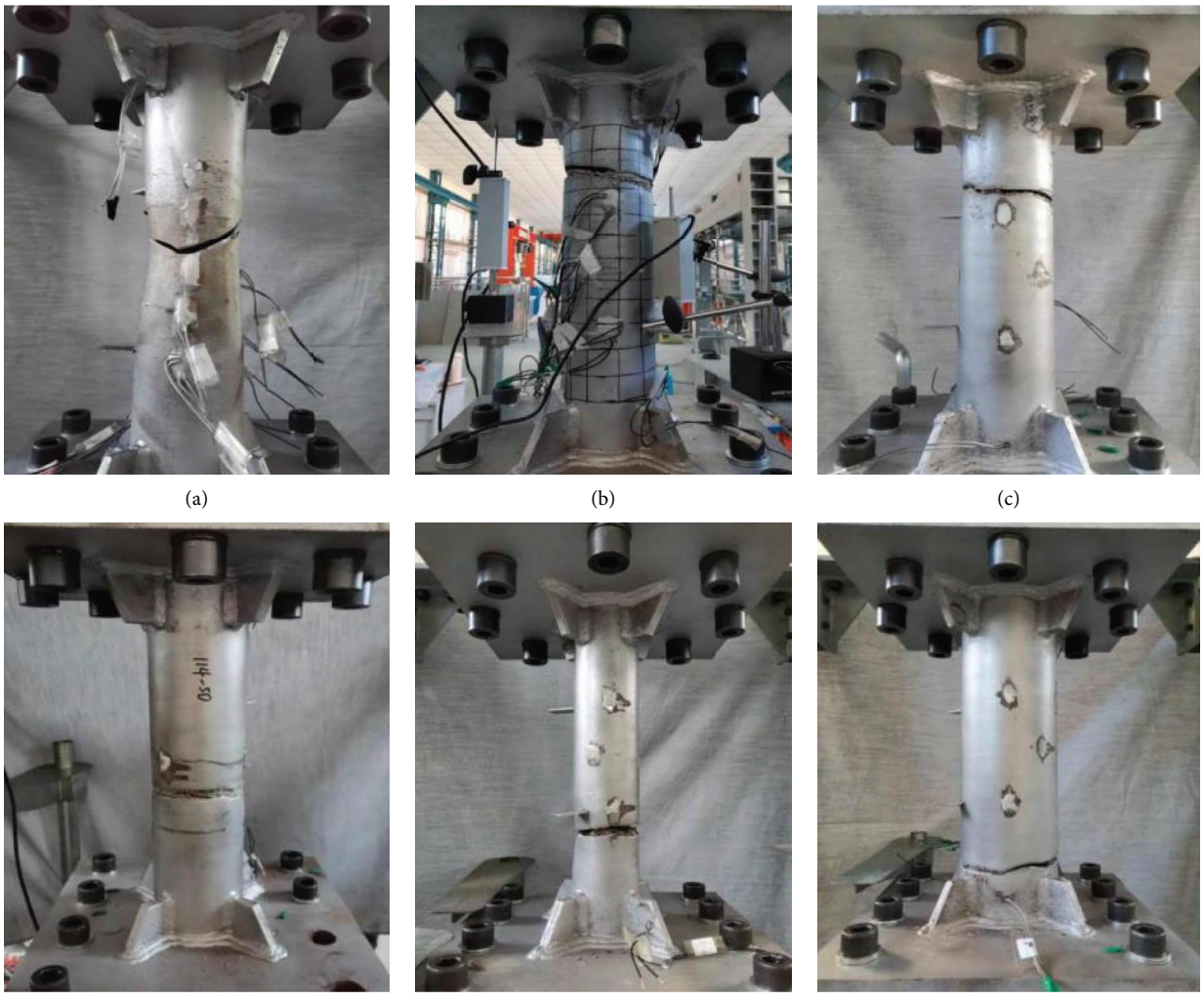

(a) (b) (c)

(d) (e) (f)

Figure 9: Damage of specimens: (a) 114-0, (b) 114-40, (c) 114-30, (d) 114-50, (e) 89-40, and (f) 139-40.

3.2. Analysis of Measured Curves

3.2.1. Load-Displacement Curve. Figure 10 shows the load-overall displacement curves of specimens 114-0 and 114-40. It can be seen from the figure that, due to the existence of core concrete, the CFST specimen has an increased bearing capacity compared with the pure steel pipe specimen of the same cross-sectional size, and the initial stiffness is greater. However, the overall ductility of the specimen is lower than that of the pure steel pipe specimen. This is because under the action of core concrete, the necking behavior of steel pipe is delayed, which leads to the decrease of ductility.

Figure 11 shows the comparison of load-relative displacement curves of concrete-filled steel tube specimens with different outer diameters and concrete strengths. It can be seen from the figure that the larger the outer diameter, the higher the bearing capacity of the specimen, and the greater the initial stiffness. With the change of concrete strength, the curves basically coincide. It can be seen that the concrete strength has a small influence on the axial tensile performance of the specimen and can be ignored.

3.2.2. Assumption of Flat Section. Figure 12 is the relationship curve between the transverse and longitudinal strain values (ε_x and ε_y) and the axial force (N) at different measuring points at the midspan section of the test piece. It can be seen from the figure that the longitudinal strain value is positive and the transverse strain value is negative. The strain-load curves in the same direction at different measuring points basically coincide, indicating that the deformation of the specimen conforms to the assumption of a flat section, and the deformation at each point of the specimen on the same cross section is consistent. And it can be seen from the figure that after adding concrete, under the same axial force, the lateral deformation of the specimen is much smaller than the longitudinal deformation. It can be seen that the concrete hinders the circumferential deformation of the outer steel pipe.

3.2.3. Strain Comparison of Inner and Outer Walls of Steel Pipe. Figure 13 shows the strain comparison between the inner and outer walls of the steel pipe of the typical specimen 139-40. As can be seen from the figure, the strain value on the inner wall of the steel pipe 1/3L away from the upper plate of the specimen is slightly smaller than that on the outer surface of the specimen. The reason is that the outer diameter of the steel pipe is larger than the inner diameter of the steel pipe, resulting in larger strain on the outer steel pipe.

3.2.4. Comparison of Deformation of Middle Section and 1/3L Section. Figure 14 shows the relationship between the ratio of the longitudinal strain (ε_y) of the middle section of the typical specimen 114-0 and 114-30 to the longitudinal strain (ε_{Uy} and ε_{Dy}) at the upper and lower 1/3L sections of the coaxial load (N) curve. It can be seen from Figure 14(a) that the shapes of the two curves are basically the same, and the abscissa values of most areas are greater than 1, indicating that the deformation at the upper and lower 1/3L sections of the test piece is basically the same. The longitudinal strain is large, so the specimen is broken in the middle section. As shown in Figure 14(b), the ratio of the longitudinal strain at the middle section to the longitudinal strain at the upper 1/3L is greater than 1, and the ratio of the longitudinal strain at the lower 1/3L section is less than 1, indicating that the specimen at the upper 1/3L deforms greatly, so the specimen failure occurred near the upper 1/3L section. The rest of the test pieces will not be repeated.

3.2.5. Deformation of Stiffener. Figure 15 shows the relationship curve between longitudinal strain and load on the stiffener of some specimens. Due to the large stiffness at the position of the stiffener, the deformation is small, resulting in irregular strain data of some specimens. Therefore, only the relationship curve of the regular specimen is listed in the figure. It can be seen that the maximum longitudinal strain of the stiffener is only 400 $\mu\varepsilon$, which is much smaller than the overall longitudinal strain value of the test piece, so the deformation of the stiffener is basically negligible.

3.3. Analysis of Bearing Capacity. Yao [19], Han [1], and Li et al. [8] have defined the method for calculating the axial tensile bearing capacity of concrete-filled steel tube specimens. The axial tensile load N_{u10000} of the concrete-filled steel tube specimen when the longitudinal strain reaches 10000 $\mu\varepsilon$ is used as the axial tensile bearing capacity of the specimen. At the same time, according to the calculation formula (1) of the CFST member axial tensile bearing capacity in the literature [7], the bearing capacity of this test specimen is calculated, and the measured bearing capacity and the formula calculated bearing capacity are listed in Table 6 and analyzed the error between the two methods.

It can be seen from the table that the measured bearing capacity is greater than the value calculated by the formula, and the error is between 14.9%–33%. It can be seen that the calculation result of formula (1) has a high safety reserve value. And it can be seen from the table that the smaller the outer diameter, the greater the error between the measured bearing capacity and the calculated bearing capacity, and with the change of concrete strength, the bearing capacity error is basically stable at about 17%.

4. Finite Element Analysis

4.1. Choice of Constitutive Relationship. The constitutive relationship of steel is mostly defined by the five-segment secondary plastic flow model proposed by Han [1]. However, it can be seen from the related test curves in the journal

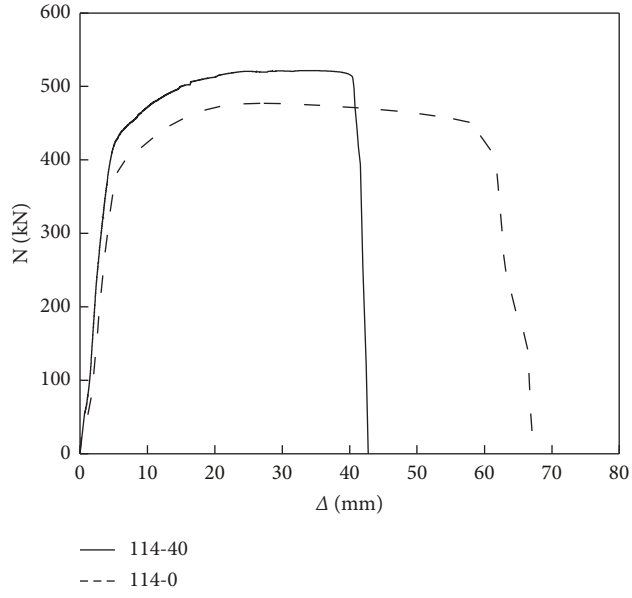

Figure 10: Load-overall displacement curve.

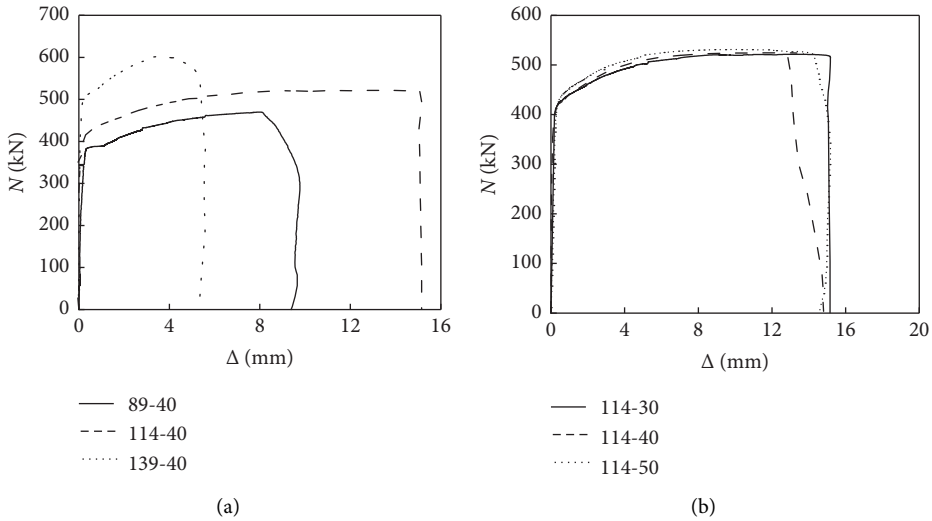

Figure 11: Load-relative displacement curve: (a) different outer diameter and (b) different concrete grades.

papers Ying [5] and Xu [20] as well as the load-displacement curve of the specimen 114-0 in Figure 8 of this paper, that the tensile stress-strain curve of steel pipe is not a clear yielding platform appears, and the material directly enters the strengthening stage after the elastic stage ends. Therefore, in order to be closer to the real material properties of the steel pipe, the secondary plastic flow model curve is adjusted accordingly as shown in Figure 16.

After removing the yield stage (bc) in the figure, the curve directly enters the strengthening stage (cd). After the modification, the constitutive relationship curve becomes a four-segment line (0abde), which is more in line with the axial tensile material properties of the pipe. The expression of the four-segment constitutive relation of steel is shown in formula (4). Among them, $\varepsilon_e = 0.8f_y/E_s$, $\varepsilon_{e1} = 1.5\varepsilon_e$, and $\varepsilon_{e2} = 100\varepsilon_{e1}$, and other parameters are consistent with the calculation method in the steel secondary plastic flow model, refer to references for values.

$$\sigma = \begin{cases} E_s\varepsilon, & (\varepsilon \le \varepsilon_e), \\ -A\varepsilon^2 + B\varepsilon + C, & (\varepsilon_e < \varepsilon \le \varepsilon_{e1}), \\ \left(1 + 0.6\dfrac{\varepsilon - \varepsilon_{e1}}{\varepsilon_{e2} - \varepsilon_{e1}}\right), & (\varepsilon_{e1} < \varepsilon \le \varepsilon_{e2}), \\ 1.6f_y, & (\varepsilon > \varepsilon_{e2}). \end{cases} \tag{4}$$

Concrete is divided into two kinds of constitutive relations of compression and tension. Compression constitutive relations are defined by the constitutive relation model

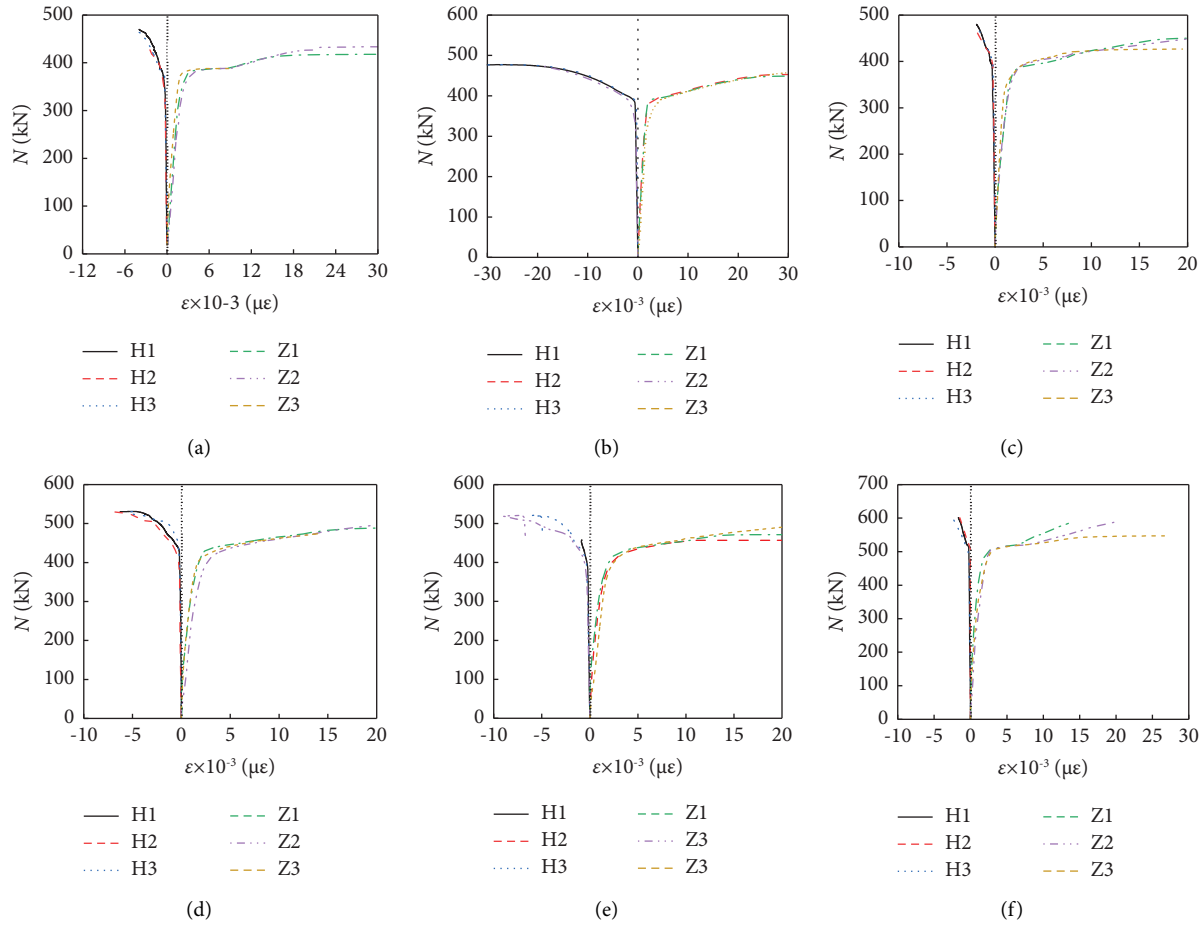

Figure 12: Flat section assumption: (a) 89-40, (b) 114-0, (c) 114-30, (d) 114-40, (e) 114-50, and (f) 139-40.

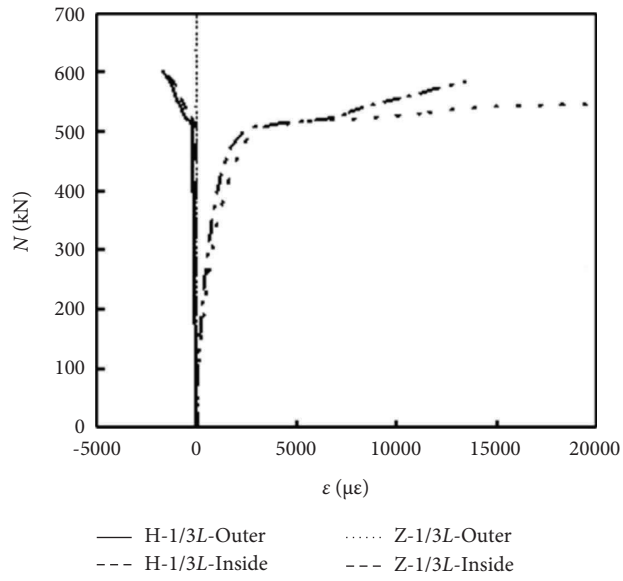

Figure 13: Strain comparison of inner and outer wall of steel pipe.

proposed by Han [1], and tension constitutive is defined by the fracture energy (GFI) module by Wang [21]. In this way, the influence of core concrete on the tensile properties of CFST members is not ignored, and the model is not prone to calculation errors due to convergence problems during the calculation process.

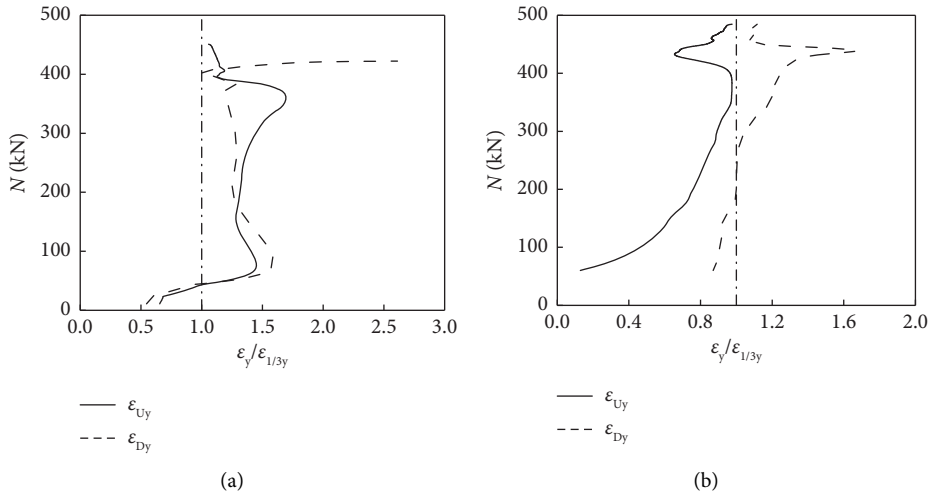

Figure 14: $\varepsilon_y/\varepsilon_{Uy}$ and $\varepsilon_y/\varepsilon_{Dy}$ with N curve: (a) 114-0 and (b) 114-30.

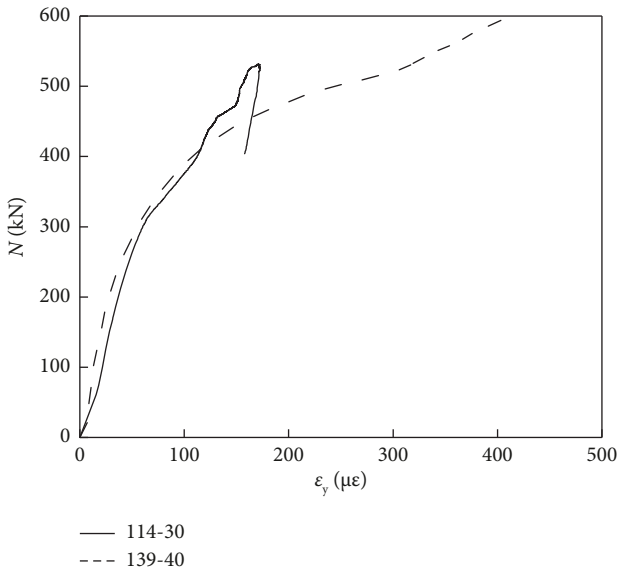

Figure 15: Curve of ε_y and N on stiffener.

Table 6: Bearing capacity comparison table.

Number	N_{u10000} (kN)	N_u (kN)	$\lvert N_{u10000} - N_u \rvert / N_{u10000}$
89-40	393.45	295.78	33.0%
114-30	449.17	388.69	15.5%
114-40	455.76	388.69	17.2%
114-50	465.58	388.69	19.7%
139-40	553.35	481.29	14.9%

4.2. Model Establishment. In order to improve the calculation accuracy and make the calculation results closer to the test results, in this paper, the finite element software ABAQUS is used to simulate the test specimen, and all components are modeled by C3D8R units. And use sweep method to mesh each part. In order to avoid distortion of the unit grid during the calculation process, the grids of all components are divided into hexahedral units, and the necessary parts are partitioned.

The choice of contact method refers to the related method in journal written by Han [1] where the contact between steel pipe and concrete is defined by surface-to-surface contact. The normal direction is "hard contact," the tangential direction is defined as "penalty," and the friction coefficient μ is 0.6. The remaining contacts are all connected by "Tie." The reference point and the end plate are connected together by coupling.

The choice of boundary conditions is consistent with the actual boundary conditions of the experiment; that is, one end is completely fixed, and the other end is loaded with displacement. The boundary conditions are shown in Figure 17.

4.3. Model Verification. Using the above modeling method and constitutive relationship, simulation calculations were carried out on 6 test specimens. Figure 18 shows the comparison of the test correlation curve of each specimen with the simulated curve. It can be seen from the figure that the curves are in good agreement. The results indicated that the model calculation results can accurately reflect the actual failure of the specimen and can be used for further failure mechanisms.

4.4. Parameter Analysis. In order to deeply understand the influence of various parameters on the axial tensile performance of CFST components, on the basis of the verification of the finite element model, the CFST axial tensile specimen was simulated with variable parameters. A total of 7 axial tension finite element models have been established. The basic parameters of the models are shown in Table 7. The external diameter of all models in Table 7 is 120 mm, and the length of the test piece is 460 mm. In the simulation process, the end plate is set as a rigid plate, and the size is 200 mm × 200 mm × 25 mm. In order to simplify the calculation, the model is not provided with stiffeners.

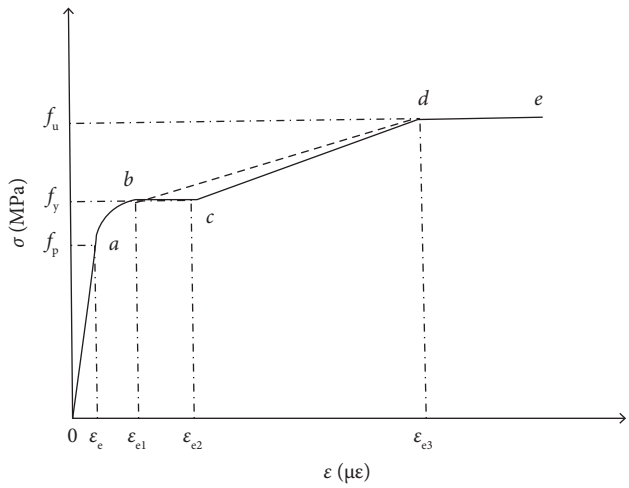

Figure 16: Adjustment of steel constitutive relationship.

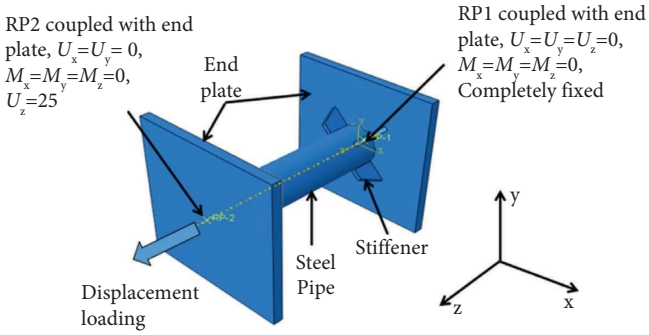

Figure 17: Boundary conditions.

Figure 19(a) is the N-ε curve of the specimens with different steel content. It can be seen that with the increase of the steel content, the load-bearing capacity of the component and the slope of the elastic phase are significantly increased, and the early stiffness of the specimen is improved. Figure 19(b) shows the comparison between the load N_{u10000} and the yield load N_{sy} of the steel pipe with the same section size when the nominal tensile strain of the specimens with different α is 10000 $\mu\varepsilon$. It can be seen that when α is 0.07, the bearing capacity is increased by 24.6%, and when the steel content is 0.19, the bearing capacity is increased by 20.9%. It can be seen that the smaller the steel content, the thinner the steel pipe wall, the more obvious the restraint effect of concrete, and the better the combination effect. In the table, A, B, and C in the number are used to distinguish the $f_{cu\cdot k}$ value, the second Arabic numerals 1, 2, and 3 are used to distinguish the f_y value, and the last number is the wall thickness t_s of the steel pipe.

Figure 20(a) shows the N-ε curve of different steel strength specimens. It can be seen that the higher the steel f_y value, the greater the bearing capacity of the specimen. The curves in the early stage of the test basically coincide, indicating that changing the f_y value of the steel does not affect the early stiffness of the specimen. The f_y value increased from 234 MPa to 420 MPa, and the component N_{u10000} value increased from 369.2 kN to 627.9 kN, an increase of 70.07%. Figure 20(b) shows the N-ε curves of different concrete strength specimens. It can be seen that the simulation results are the same as the test results; that is, the three curves basically overlap. It shows that concrete is not the main factor affecting the axial tensile performance of CFST members.

4.5. Simplified Calculation of Bearing Capacity. At present, the calculation formulas in domestic and foreign codes do not consider the influence of concrete and only introduce correlation coefficients based on the tensile strength of steel sections. Foreign standards reduce the tensile strength of steel sections, while domestic standards increase the coefficient of improvement by 1.1 times. Formula (1) essentially increases the improvement factor related to the steel content. In this paper, a total of 25 axial tension specimens including the test specimens are simulated and calculated. The relevant parameters of all specimens are shown in Table 8.

On the basis of a large number of finite element calculations, a formula for calculating the axial tensile bearing capacity related to the ratio of the wall thickness to the diameter of the steel pipe (t_s/D) is proposed, and t_s/D is defined as "λ," and the formula is obtained by referring to formula (5) as follows:

$$N_u = (1 + B\lambda)A_s f_y. \tag{5}$$

It can be seen that the bearing capacity N_u and "λ" are linear functions. By shifting the terms of the above formula, the formula (6) is obtained as follows:

$$N_u - A_s f_y = B \cdot A_s f_y \lambda, \tag{6}$$

where N_u is the axial tension capacity, A_s is the cross-sectional area of the steel tube, f_y is the yield strength of steel tube, B is the slope of the first order function, and λ is the ratio of steel tube wall thickness to diameter.

After fitting the bearing capacity, as shown in Figure 21, the slope and intercept values are 8.09 and 5.549, respectively. From a safety point of view, the intercept can be omitted, and the final bearing capacity calculation formula is as follows:

$$N_u = (1 + 8.09\lambda)A_s f_y. \tag{7}$$

Since the steel content of the finite element specimen used for fitting is between 0.041 and 0.19, this formula is only applicable to CFST members with steel content between 0.041 and 0.19.

4.6. Verification of the Axial Tension Formula. Formula (7) is used to calculate the bearing capacity of 5 concrete-filled steel tube specimens in this test. Figures 22(a) and 22(b) show the comparison of the bearing capacity of the two. The calculation shows that the calculation result of the formula is 10000 $\mu\varepsilon$. The error of the bearing capacity is between 1.3%–3.8%, and the error of the ultimate bearing capacity measured in the test is between 15.1% and 24.7%. Therefore, the

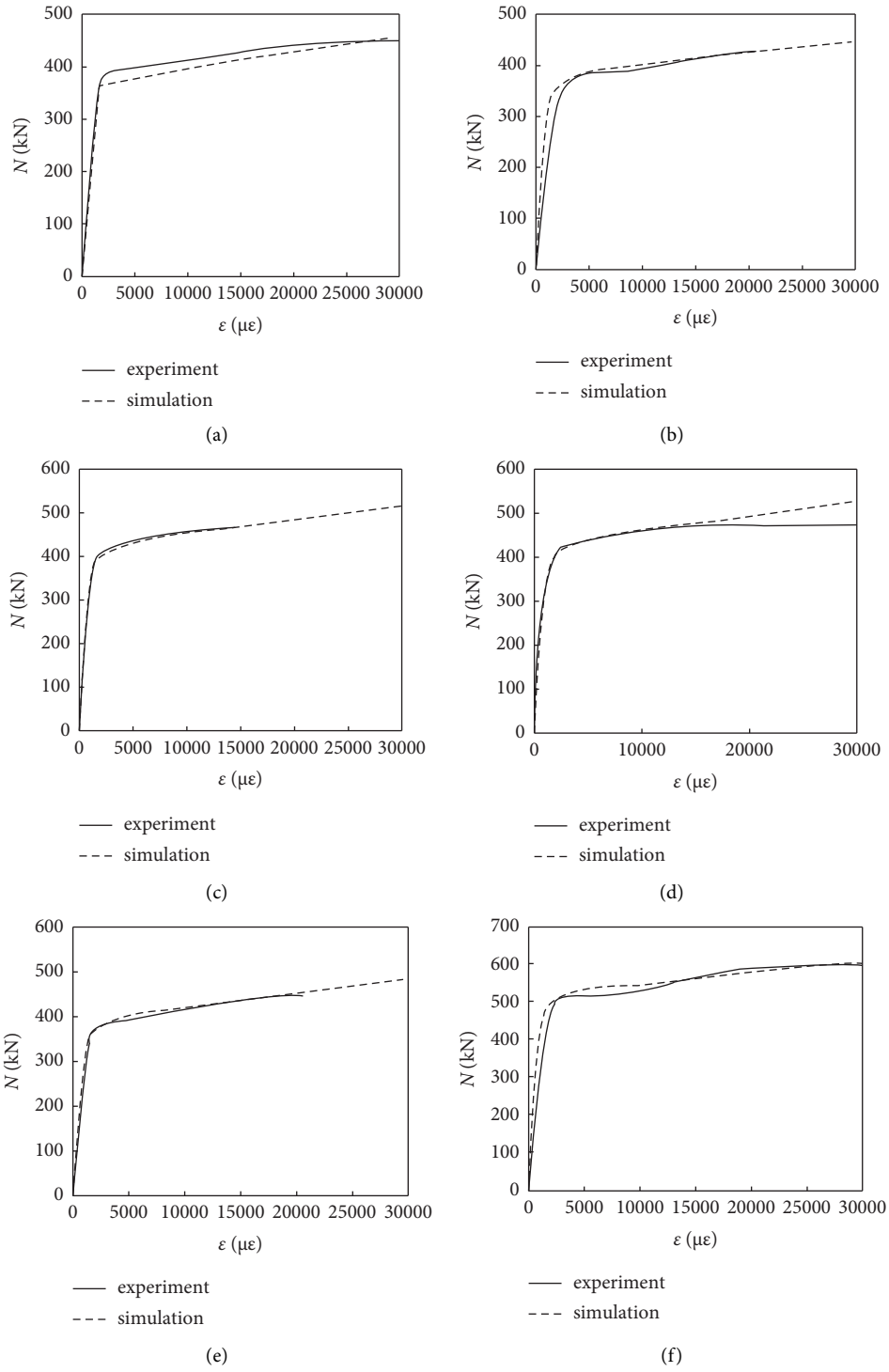

Figure 18: Comparison of test results and finite element calculation results: (a)114-0, (b) 89-40, (c) 114-30, (d) 114-40, (e) 114-50, and (f) 139-40.

Table 7: Simulation test piece parameters.

Number	Serial number	t_s (mm)	α	f_y (MPa)	$f_{cu\cdot k}$ (MPa)
1	A1-3.5	3.5	0.13	235	30
2	B1-3.5	3.5	0.13	235	40
3	C1-3.5	3.5	0.13	235	50
4	A1-2	2	0.07	235	30
5	A1-5	5	0.19	235	30
6	A2-3.5	3.5	0.13	345	30
7	A3-3.5	3.5	0.13	420	30

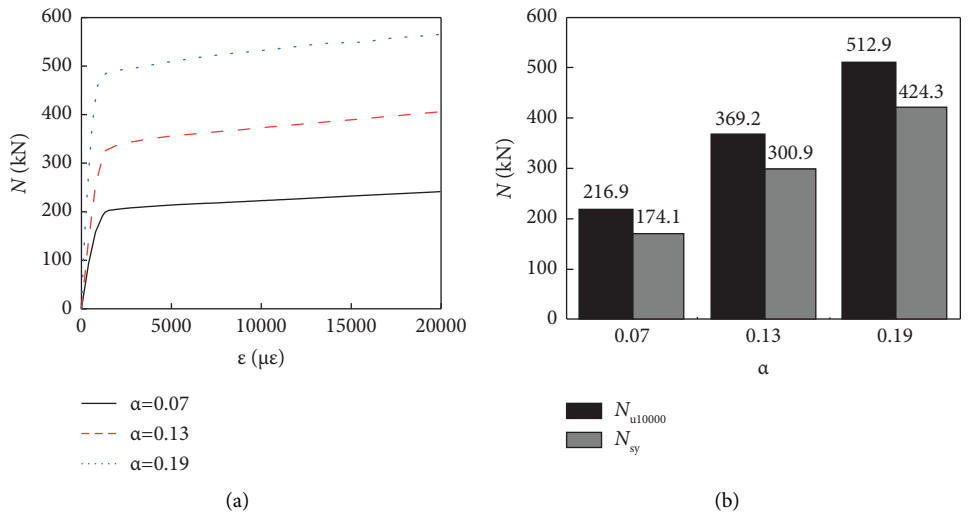

Figure 19: The influence of α on the axial tensile properties: (a) N-ε curve of specimen under different α and (b) comparison of N_{u10000} and N_{sy} under different α.

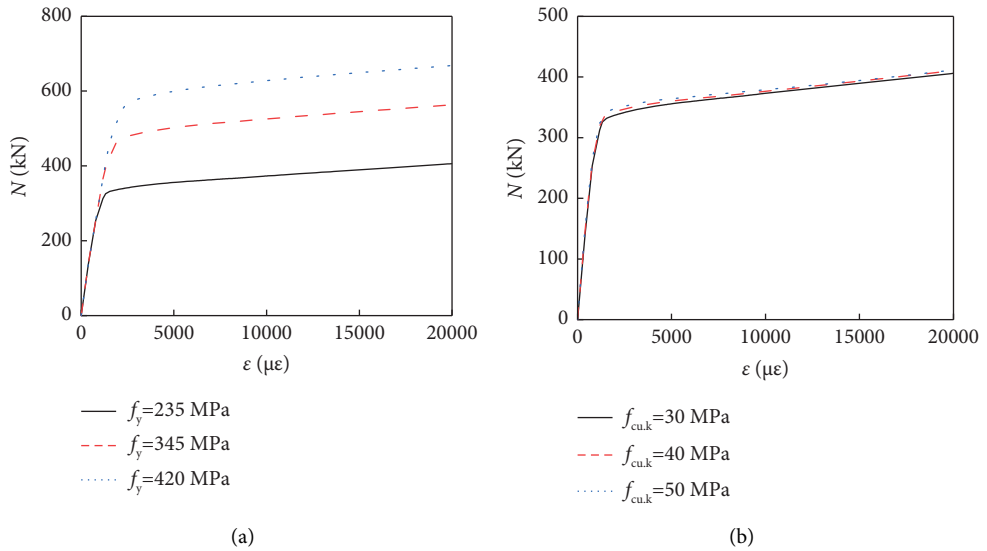

Figure 20: The influence of f_y and $f_{cu\cdot k}$ on the axial tensile properties: (a) N-ε curve of specimen under different f_y and (b) N-ε curve of specimen under different $f_{cu\cdot k}$.

Table 8: Simulation model summary.

Number	Number	$t_s \times D$ (mm)	α	f_y (MPa)	$f_{cu \cdot k}$ (MPa)
1	89-40	3.5×89	0.178	306	40
2	114-40	3.5×114	0.135	306	40
3	139-40	3.5×139	0.109	306	40
4	114-30	3.5×114	0.135	306	30
5	114-50	3.5×114	0.135	306	50
6	A1-3.5	3.5×120	0.13	235	30
7	B1-3.5	3.5×120	0.13	235	40
8	C1-3.5	3.5×120	0.13	235	50
9	A1-2	2×120	0.07	235	30
10	A1-5	5×120	0.19	235	30
11	A2-3.5	3.5×120	0.13	345	30
12	A3-3.5	3.5×120	0.13	420	30
13	235-40-1	1×40	0.108	235	30
14	235-50-1	1×50	0.085	235	30
15	235-60-1	1×60	0.07	235	30
16	235-50-0.5	0.5×50	0.041	235	30
17	235-50-1.5	1.5×50	0.132	235	30
18	345-50-1	1×50	0.085	345	30
19	420-50-1	1×50	0.085	420	30
20	235-220-4	4×220	0.077	235	30
21	235-220-5	5×220	0.097	235	30
22	235-220-6	6×220	0.119	235	30
23	235-200-5	5×200	0.108	235	30
24	235-240-5	5×240	0.089	235	30

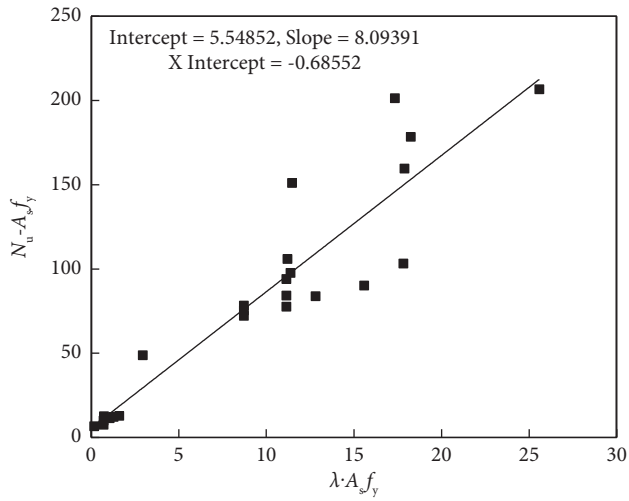

Figure 21: Axial pull formula fitting curve.

calculation accuracy of the formula is high, and it has a high safety reserve value.

Compare the N_{u10000} test values of 6 typical CFST axial tensile test specimens with the calculated results of the formula in documents Wang [21], Han [1], Wang [22], Hua et al. [4]. The comparison is shown in Figure 23. It can be seen that the two values are basically the same. The smaller the outer diameter of the steel pipe, the smaller the error. And the bearing capacity value calculated by the formula is slightly smaller than the value of N_{u10000} measured in the experiment, and the error is between 9.1%–13.1%. It can be seen that the bearing capacity calculated by formula (6) is accurate and reliable.

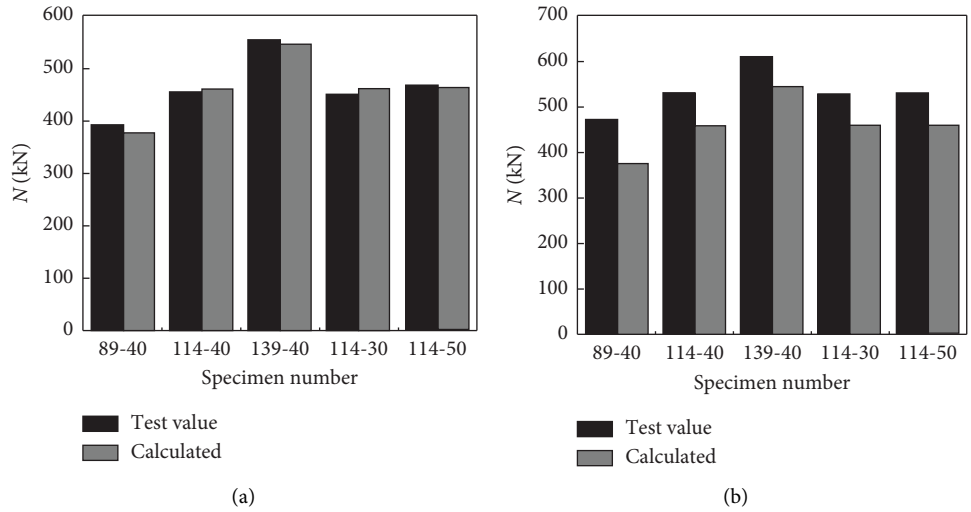

Figure 22: Comparison of measured bearing capacity and calculated bearing capacity: (a) N_{u10000} test value and calculated value comparison and (b) comparison of test ultimate bearing capacity and calculated value.

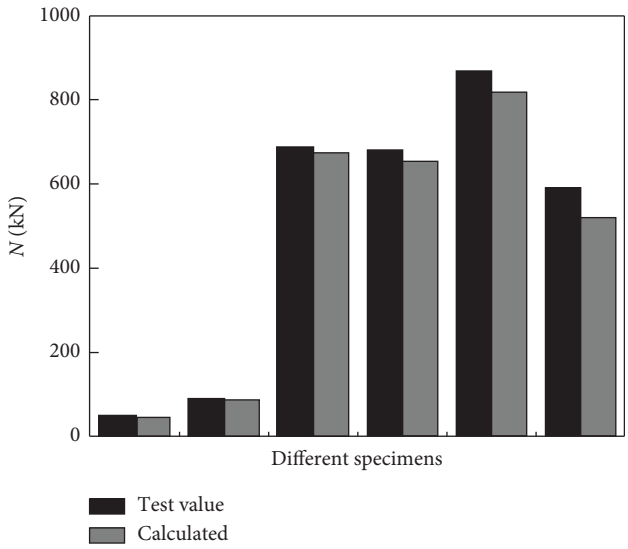

Figure 23: Comparison of the measured bearing capacity of the specimen in the literature and the calculated value of the formula.

5. Conclusions

(i) The failure section of the pure steel pipe specimen appears at the midspan section position, while the failure position of the CFST specimen occurs near the 1/3L section and where the top of the stiffener contacts the steel pipe.

(ii) The reason for the increase in the bearing capacity of the CFST specimen is that the core concrete limits the circumferential shrinkage of the outer steel pipe, and the increase is between 7.5% and 16.3%. However, the ductility of CFST specimens is slightly worse than that of pure steel pipe specimens.

(iii) Compared with the tensile stress-strain curve of steel pipe and steel plate, there is no yield platform, so the five-segment secondary plastic flow model is adjusted. The simulated calculation results of the adjusted steel constitutive relationship are in good agreement with the test results.

(iv) Through the analysis of the test and finite element method parameters, the higher the steel content, the greater the early stiffness of the specimen, and the higher the bearing capacity, but the worse the effect of the combination of steel pipe and concrete. The increase in steel strength does not change the specimen. The initial stiffness can effectively improve the bearing capacity; concrete is not the main factor that affects the axial tensile performance of CFST specimens.

(v) A simplified calculation formula for the axial tension bearing capacity related to t_s/D is

suggested. The error between the calculated result of the formula and the measured value of N_{u10000} is between 1.3% and 3.8%, which is 15.1%–24.7 compared with the measured ultimate bearing capacity. The safety reserve value can provide a reference for quickly calculating the bearing capacity of this type of member in actual engineering.

(vi) When the connection between the concrete and the steel wall is failed, the friction between the concrete and the outer steel pipe will be generated when under tension, and the axial tension will be transmitted to the core concrete through the friction. When the concrete reaches the ultimate tensile stress, the concrete is pulled off (at 1/3L), the friction between the two at the pull off position disappears, the radial support effect of the core concrete on the steel pipe disappears, and the steel pipe necks here until it is damaged. However, there is still friction between the outer steel pipe and the core concrete at the unbroken position, and the concrete still plays the role of internal support.

(vii) For various reasons, this paper only carried out the axial tension test of CFST specimens, but the eccentric tension test of CFST members was not carried out. Therefore, it is suggested to carry out the eccentric tension test and compare the test results with the theoretical results. At present, there are relatively few experimental studies on eccentrically tensioned concrete-filled steel tubular members, and the system is still not perfect. Therefore, it is necessary to carry out relevant eccentric tension experimental studies.

(viii) In harsh environment, it will also cause corrosion of steel pipes outside CFST members, so it is necessary to study the tensile properties of corroded CFST members. At the same time, in order to study the tensile properties of strengthened CFST members, it is recommended to study the tensile properties of CFST specimens under different reinforcement methods, such as CFRP reinforcement and steel clad reinforcement.

(ix) In order to better solve the problem of separation from the outer steel tube during concrete curing, it is suggested to use microexpansive concrete, such as adding magnesium oxide powder expansion agent, to study the influence of the bonding force between steel tube and concrete on the axial tensile properties of CFST specimens.

Data Availability

The data supporting the current study are available from the corresponding author upon request.

Conflicts of Interest

The authors declare that they have no conflicts of interest.

Acknowledgments

This work was partially supported by the General Project of the Natural Science Foundation of China (Grant no. 51678542) and the Project of Revitalizing Liaoning Talents (Grant no. XLYC1902009).

References

[1] L. H. Han, *Concrete Filled Steel Tubular Structures - Theory and Practice*, Science Press, Beijing, China, 3rd edition, 2016.

[2] M. Zhou, J. S. Fan, M. X. Tao, and J. G. Nie, "Experimental study on the tensile behavior of square concrete-filled steel tubes," *Journal of Constructional Steel Research*, vol. 121, pp. 202–215, 2016.

[3] L. Y. Xu, M. X. Tao, and M. Zhou, "Analytical model and design formulae of circular CFSTs under axial tension," *Journal of Constructional Steel Research*, vol. 133, pp. 214–230, 2017.

[4] Y. X. Hua, C. Hou, and L. H. Han, "Behaviour of CFST tensile members subjected to chloride corrosion," *Engineering Mechanics*, vol. 32, no. 1, pp. 149–152+158, 2015.

[5] Z. Ying, *Experimental Study on Mechanical Properties of RPC-FST under Direct Tension load*, Fujian Agriculture and Forestry University, Fuzhou, China, 2016.

[6] J. Wang, Y. Liu, X. Guo, B. Dong, and Y. Cao, "High-level expression of lipase from Galactomyces geotrichum mafic-0601 by codon optimization in Pichia pastoris and its application in hydrolysis of various oils," *3 Biotech*, vol. 9, no. 10, pp. 354–361, 2019.

[7] L. H. Han, Z. B. Wang, W. Xu, and Z. Tao, "Behavior of concrete-encased CFST members under axial tension," *Journal of Structural Engineering*, vol. 142, no. 2, Article ID 4015149, 2016.

[8] W. Li, L. H. Han, and T. M. Chan, "Performance of concrete-filled steel tubes subjected to eccentric tension," *Journal of Structural Engineering*, vol. 141, no. 12, Article ID 4015049, 2015.

[9] Z. B. Wang, Q. Yu, and Z. Tao, "Behaviour of CFRP externally-reinforced circular CFST members under combined tension and bending," *Journal of Constructional Steel Research*, vol. 106, pp. 122–137, 2015.

[10] W. Li, L. H. Han, and T. M. Chan, "Numerical investigation on the performance of concrete-filled double-skin steel tubular members under tension," *Thin-Walled Structures*, vol. 79, pp. 108–118, 2014.

[11] J. Chen, J. Wang, and W. L. Jin, "Experimental investigation on concrete-filled steel tubes with reinforcing bars under axial and eccentric tension," *Journal of Building Structures*, vol. 38, no. 1, pp. 272–277, 2017.

[12] Y. Ye, W. Li, X. J. Liu, and Z. X. Guo, "Behaviour of concrete-filled steel tubes with concrete imperfection under axial tension," *Magazine of Concrete Research*, vol. 73, no. 14, pp. 743–756, 2021.

[13] L.-H. Han, S. H. He, and F. Y. Liao, "Performance and calculations of concrete filled steel tubes (CFST) under axial tension," *Journal of Constructional Steel Research*, vol. 67, no. 11, pp. 1699–1709, 2011.

[14] J. Chen, J. Wang, and W. L. Jin, "Concrete-filled steel tubes with reinforcing bars or angles under axial tension," *Journal of Constructional Steel Research*, vol. 133, pp. 374–382, 2017b.

[15] M. Zhou, L. Y. Xu, M. X. Tao, J. S. Fan, J. F. Hajjar, and J. G. Nie, "Experimental study on confining-strengthening, confining-stiffening, and fractal cracking of circular concrete

filled steel tubes under axial tension," *Engineering Structures*, vol. 133, pp. 186–199, 2017.

[16] Q. Qiao, X. Li, W. Cao, and H. Dong, "Seismic behavior of specially shaped concrete-filled steel tube columns with multiple cavities," *The Structural Design of Tall and Special Buildings*, vol. 27, no. 12, pp. 14855–1515, 2018.

[17] GB/T2281, *Tensile Test of Metallic Materials Part 1: Tensile Method at Room Temperature*, Ministry of Housing and Urban-Rural Development, Beijing, China, 2011.

[18] GB/T50081, *Standard for Test Methods of Physical and Mechanical Properties of Concrete*, Ministry of Housing and Urban-Rural Development, Beijing, China, 2019.

[19] G. H. Yao, *Research on Behaviour of Concrete-filled Steel Tubes Subjected to Complicated Loading states*, Fuzhou University, Fuzhou, China, 2006.

[20] X. C. Xu, *Study on Behavior of CFRP Strengthen concrete-filled Steel Tube under Eccentric tension*, Fuzhou University, Fuzhou, China, 2013.

[21] Q. L. Wang, *CFRP - Concrete-filled Steel Tube*, Science Press, Beijing, China, 2017.

[22] L. B. Wang, *Research on Tensile Bearing Capacity and Beams-Columns Hysteretic Behaviour of Concrete-Filled Stainless Steel Tubes*, Fuzhou University, Fuzhou, China, 2011.